Russian Journal of Earth Sciences Online ISSN: 1681-1208

Special Issue: "Kamchatka Earthquake M 8.8 on July 29, 2025"

Ionospheric Response to the Seismic Wave Induced by the Kamchatka Earthquake on July 29, 2025

A. V. Oinats*[,1], M. V. Cedrik[1], I. Yu. Dyukov[1], A. V. Podlesny[1], A. Yu. Belinskaya[2], A. A. Borovko[2], A. G. Sorokin[1], V. A. Dobrynin[1], and P. A. Dergach[2]

[1] Institute of Solar-Terrestrial Physics Siberian Branch of the Russian Academy of Sciences, Irkutsk, Russian Federation

[2] Trofimuk Institute of Petroleum Geology and Geophysics Siberian Branch of the Russian Academy of Sciences, Novosibirsk, Russian Federation

* **Correspondence to:** Alexey Oinats, oinats@iszf.irk.ru

Abstract: The July 29, 2025 earthquake near the eastern coast of the Kamchatka Peninsula induced a high-amplitude seismic wave that propagated thousands of kilometers from the epicenter. Ground vibrations caused variations in surface air pressure with periods in the infrasonic range, which propagated almost vertically into the upper atmosphere and modulated the ionospheric plasma. The resulting ionospheric disturbances were, in turn, recorded by a number of radiophysical facilities monitoring the ionosphere. In this paper, we provide an overview of the effects caused by the passage of the seismic wave, which were observed during ionospheric monitoring using vertical, oblique, and sky-wave backscatter sounding techniques in the Asian part of Russia.

Keywords: Lithosphere-atmosphere-ionosphere coupling, ionosphere monitoring, vertical sounding, oblique sounding, sky-wave backscatter sounding, HF radar, infrasound, Kamchatka megathrust earthquake

Citation: Oinats A. V., Cedrik M. V., Dyukov I. Yu., Podlesny A. V., Belinskaya A. Yu., Borovko A. A., Sorokin A. G., Dobrynin V. A., and Dergach P. A. (2026), Ionospheric Response to the Seismic Wave Induced by the Kamchatka Earthquake on July 29, 2025, *Russian Journal of Earth Sciences*, 26, ES2021, EDN: CYKDQR, https://doi.org/10.2205/2026es001131

Research Article

Received: February 2, 2026
Accepted: May 25, 2026
Published: July 1, 2026

1. Introduction

The study of lithosphere-atmosphere-ionosphere coupling is of great scientific and practical importance. One manifestation of this interaction is the emergence of short-lived irregularities in the ionospheric plasma above the earthquake epicenter itself, as well as above regions where seismic waves propagate. The primary mechanism for the formation of these irregularities is the generation of an acoustic infrasound wave during oscillations of the Earth's surface, the propagation of this wave to the heights of the upper atmosphere, and the subsequent modulation of the ionospheric plasma [*Pokhotelov et al.*, 1995].

Such disturbances were first recorded after the 1964 Alaska earthquake in Doppler vertical and oblique sounding [*Davis and Baker*, 1965], and also as trace distortions on vertical ionograms [*Leonard and Jr.*, 1965]. Further development of ionospheric monitoring techniques and technology made it possible to detect such disturbances in transionospheric [*Afraimovich et al.*, 2001; *Rolland et al.*, 2011; *Tsugawa et al.*, 2011], Doppler [*Artru et al.*, 2004; *Chum et al.*, 2012, 2016], vertical [*Maruyama and Shinagawa*, 2014; *Maruyama et al.*, 2012] and sky-wave backscatter sounding [*Nishitani et al.*, 2011], as well as in a combined analysis of data from various observations [*Liu et al.*, 2016; *Ogawa et al.*, 2012].

This paper provides an overview of the effects observed in ionospheric monitoring data in the Asian part of Russia after the earthquake near the eastern coast of the Kamchatka Peninsula on July 29, 2025.

2. Data and Methods

The Kamchatka earthquake onset was recorded at 23:24 UTC on July 29, 2025. The epicenter was located at 52.47°N, 160.40°E. The moment magnitude was 8.8, and the hypocenter depth was 47 km. We present data from seismological stations in Petropavlovsk-Kamchatsky (PET), Magadan (MA2), Yakutsk (YAK), Talaya (TLY), and Novosibirsk (NSK, the Klyuchi research station). Surface excess air pressure variations were obtained at the acoustic station of the Geophysical Observatory (GO) of ISTP SB RAS in Tory (TORY). Ionospheric monitoring was carried out using vertical sounding (VS) at the GO in Tory and at the Klyuchi research station in Novosibirsk (NSK), oblique sounding (OS) – the Novosibirsk–Tory path (NSK-TORY), and sky-wave backscatter sounding (BS) by the MGW HF radar located in Stekolny near Magadan. Figure 1 shows a schematic map of the earthquake epicenter and observation stations. The solid line on the map shows the Novosibirsk–Tory oblique path. Additionally, dotted lines show the Magadan–Novosibirsk and Magadan–Tory oblique paths, as well as the MGW HF radar field of view. The coordinates of the observation stations, the type of observation, the distance, and the azimuth from the epicenter are provided in Table 1.

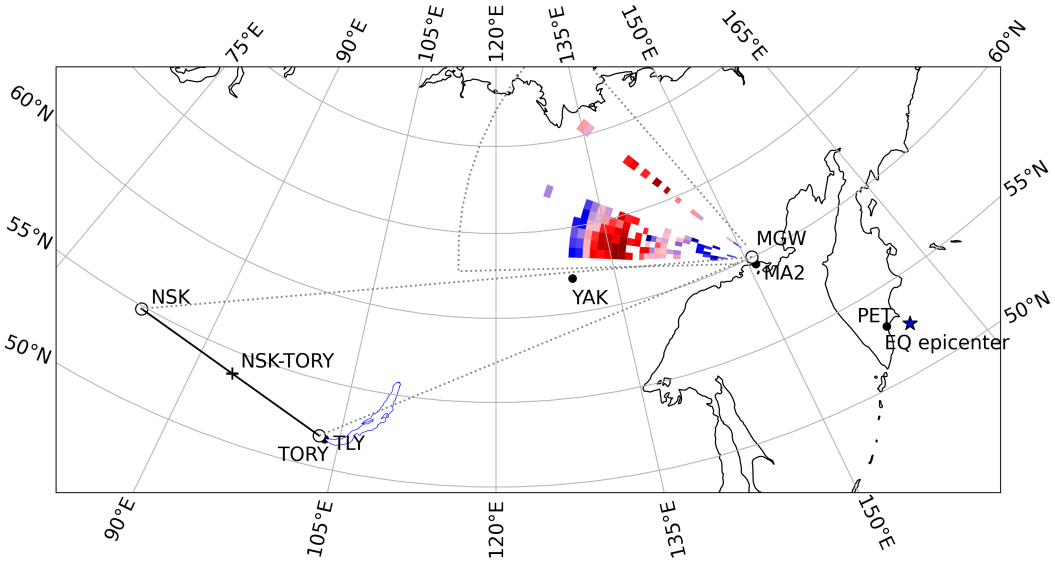

Figure 1. Map of observation station locations.

Table 1. Observation station coordinates, distance and azimuth from epicenter

No.	Station name	Type of observation	Latitude	Longitude	Distance	Azimuth
1	Petropavlovsk-Kamchatsky (PET)	seismic	53.02	158.65	132.5	298.2
2	Magadan (MA2)	seismic	59.58	150.77	988.7	326.8
3	HF radar (MGW)	BS	60.03	150.73	1028.6	328.5
4	Yakutsk (YAK)	seismic	62.03	129.69	2102.5	312.3
5	Talaya (TLY)	seismic	51.68	103.64	3777.8	291.9
6	Tory (TORY)	VS, acoustic	51.81	103.08	3807.3	292.4
7	Middle point of Novosibirsk–Tory HF path (NSK–TORY)	OS	53.74	93.51	4298.3	299.4
8	Novosibirsk (NSK)	seismic, VS	54.85	83.23	4828.2	305.2

3. Results

3.1. Correlation of Seismological and Acoustic Observations

Figure 2 shows the variations in the velocity of vertical ground motion (BHZ component) recorded at seismological stations. The variations are arranged in order of increasing distance from the epicenter, which is marked with a star in the figure. We indicate the scale of variations for each station by a vertical line next to the station name. The figure shows that vertical ground motions reached over 10 cm/s in Petropavlovsk-Kamchatsky, about 3 mm/s in Magadan, Yakutsk, and Talaya, and less than 0.1 mm/s in Novosibirsk. The approximate travel delays of the Rayleigh wave to stations MA2, YAK, TLY, and NSK were 5, 10, 20, and 25 minutes, respectively. The estimated Rayleigh wave velocity, based on its arrival at the YAK and TLY seismological stations, is approximately 3 km/s. At stations TLY and NSK, the faster P- and S-waves are also clearly distinguishable. The P-wave velocity increases with distance from the epicenter, ranging from 6.2 to 9.8 km/s. The S-wave velocity at stations TLY and NSK is about 6.5 km/s. The shape of the variations changes significantly from station to station, indicating substantial dispersion of the seismic wave.

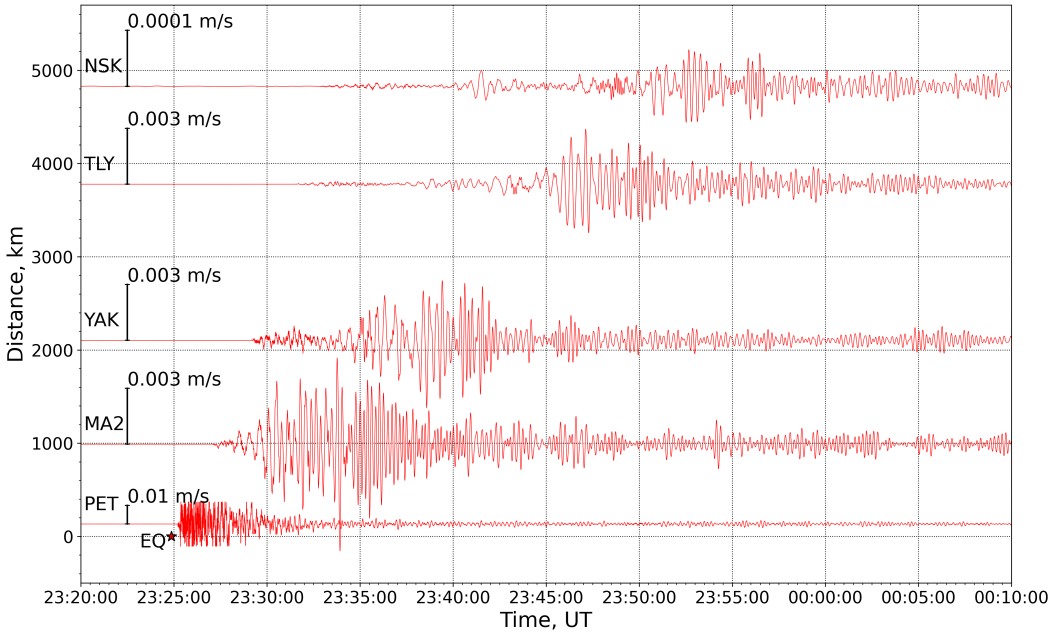

Figure 2. Velocity of vertical ground motion as recorded at seismological stations in Petropavlovsk-Kamchatsky, Magadan, Yakutsk, Talaya, and Novosibirsk from 23:20 UTC on July 29, 2025, to 00:10 UTC on July 30, 2025.

Figure 3a shows variations in excess air pressure near the surface (black line) recorded at the GO acoustic station in Tory. It is evident that, in addition to the deep background variations with periods of about 10–20 minutes, there are also oscillations with periods of 10–20 seconds. Applying bandpass filtering in the range of 0.3–50 seconds yields the variations shown by the blue line. The oscillations of excess air pressure, converted to gas velocity in a traveling acoustic wave ($v = p/(c_a\rho_a)$, where p is excess pressure, and c_a and ρ_a are the speed of sound and air density at the surface [*Lighthill*, 2001]), are presented in Figure 3b alongside the data from the Talaya seismic station. One can see that the gas velocity variations and vertical ground oscillations are in complete agreement. The delay between the gas velocity and ground oscillations, determined by the maximum of the correlation function (~0.7), is approximately 8.86 seconds. The distance between Talaya and Tory projected onto the direction of the Rayleigh wave propagation is about 29.5 km as one can conclude from Table 1. Since the Rayleigh wave (as the wave with the largest amplitude) makes the main contribution to the correlation, we estimate its velocity at about 3.3 km/s on the Talaya–Tory route.

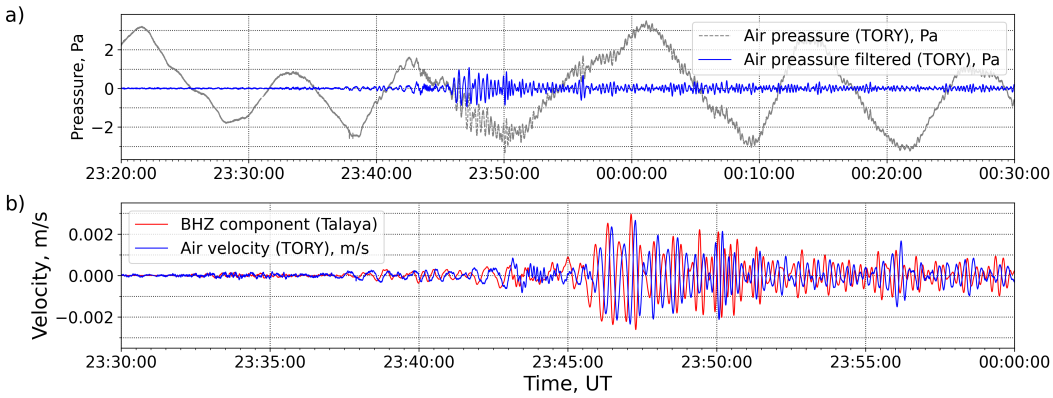

Figure 3. (a) Surface excess air pressure as recorded in Tory from 23:20 UTC on July 29, 2025, to 00:30 UTC on July 30, 2025. The black line represents the raw variations, and the blue line shows the variations after bandpass filtering in the period range of 0.3–50 seconds. (b) The red line indicates the vertical ground motion velocity at the Talaya seismic station, and the blue line represents the excess air velocity in Tory.

3.2. Doppler Velocity of Ground Scatter Observed by the MGW HF Radar

The MGW HF radar is a part of the Sekira radar network [*Berngardt et al.*, 2020] and is located in Stekolny, Magadan Region. Figure 1 shows the radar's field of view as a circular sector bounded by dotted lines. The radar monitors the ionosphere using direct ionospheric backscatter (IS) and sky-wave backscatter sounding (BS). In BS mode, HF radio waves propagate along oblique trajectories, are reflected by the ionosphere, scatter from surface roughness, and return to be recorded by the radar. Unlike classical BS, HF radars transmit radio waves at a fixed frequency.

Figure 4 presents a distance-time diagram of the Doppler velocity of the ground scatter echoes observed by beam 2 (azimuth −57°) as a function of Universal Time and ground distance. The radar operational frequency was 8.2 MHz. The temporal and spatial resolutions were 28 seconds and 45 km, respectively. The vertical axis indicates the ground distance in kilometers from the radar to the scattering point. For ground scatter echoes this distance corresponds to the apogee of the radio wave trajectory. Doppler velocity is shown by color according to the color scale on the right of the figure. The red color indicates motion of the scatter away from the radar along the beam, and the blue color indicates motion toward the radar. In the case of undisturbed, slowly changing ionosphere, the ground scatter echoes have Doppler velocities close to zero, as the ground surface itself is a stationary scattering object. This is indeed observed in Figure 4 up to 23:40 UTC. From approximately 23:40 UTC to 23:50 UTC, we can clearly see four distinct inclined bands of alternating increase and decrease in Doppler velocity, originating from the HF skip distance. The peak-to-peak amplitude of the Doppler velocity reaches ~120 m/s. The observed Doppler velocity variations are most likely associated with the passage of the radio waves through a region of moving plasma irregularities, generated by an acoustic wave traveling in the ionosphere. The delay between the onset of the earthquake and the observed effect (~15 minutes) is composed of the time required for the Rayleigh wave to reach the radar's field of view (~8 minutes) and for the acoustic wave to ascend from the ground surface to ionospheric heights at the sound speed (~7 minutes). The slope of the bands indicates that the irregularity was moving away from the radar at a speed of approximately 2 km/s as projected onto beam 2. This is confirmed by the alignment of the red bands with the black dashed lines, which correspond to a wavefront phase velocity of 1.9 km/s originating from the epicenter. It should be noted that after 23:50 UTC, pink and light blue bands are still visible in the figure, indicating the continued presence of irregularities, albeit less intense.

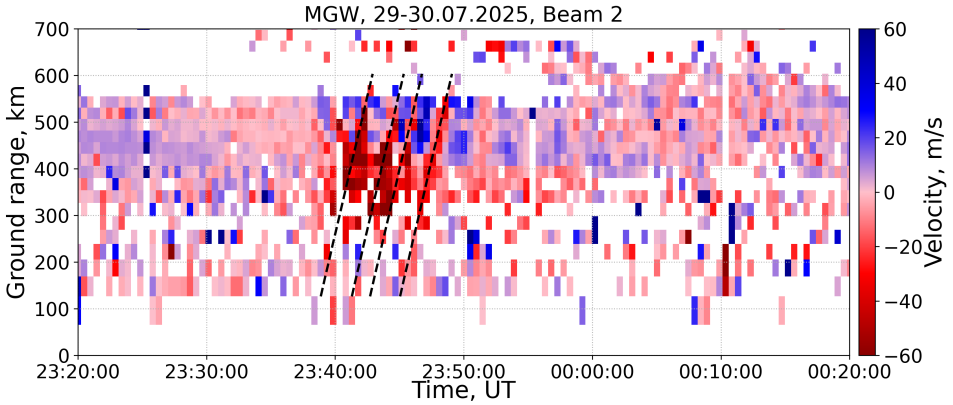

Figure 4. Doppler velocity of ground scatter as measured by the MGW HF radar beam 2.

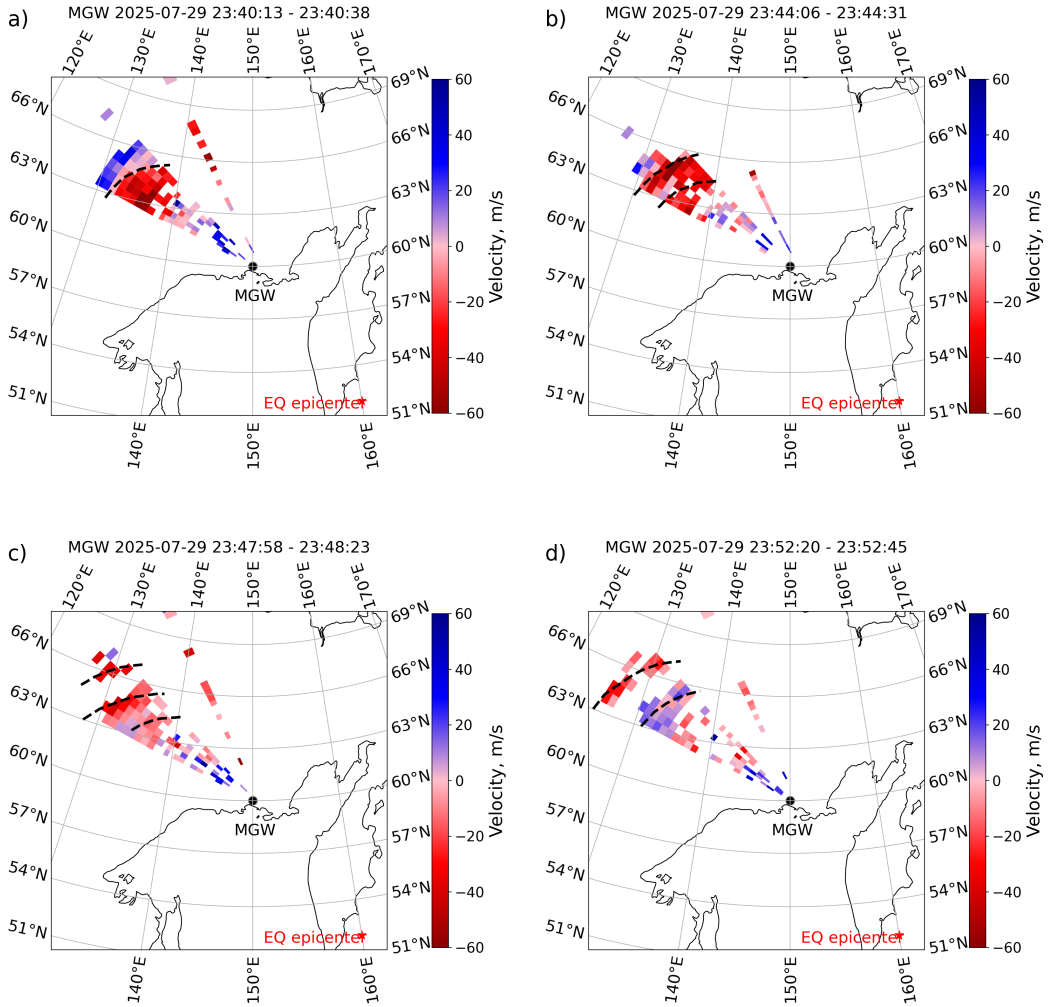

Figure 5. Doppler velocity of ground backscatter in the MGW HF radar field of view for individual scans.

Figure 5 shows the Doppler velocity distributions in the radar field of view for individual scans. During the period of interest the radar was sequentially sampling beams 12, 6, 5, . . . , 1, counterclockwise from the easternmost to the westernmost beam. The integration time was 4 seconds, so that the radar covered the whole field of view every 28 seconds. The beam sampling sequence introduces a slight distortion into the observed wavefronts, since the disturbance is moving during the sampling process. Nevertheless, the panels of Figure 5 clearly show concentric bends in the Doppler velocity, the center

of which approximately corresponds to the earthquake epicenter. For convenience the wavefronts are marked by the dashed lines on the panels. The distance between adjacent fronts is about 100–200 km. As we can see from Figure 1, the far boundary of the MGW measurement region is located near the YAK station. The approximate delay between the appearance of the Rayleigh wave at the YAK station and the onset of the main effect in the MGW HF radar data is about 7 minutes, which corresponds to the propagation duration of infrasound from the ground surface to ionospheric heights.

3.3. Distortions of the Vertical Ionograms in Tory and Novosibirsk

During the period of interest, the vertical sounding chirp ionosonde in Tory [*Podlesnyi et al.*, 2013] was operated with a time resolution of 15 seconds. This allowed a fairly detailed observation of the ionospheric effects caused by the passage of an acoustic wave generated by a seismic wave. Figure 6a shows the vertical ionogram before the onset of earthquake effects. It can be seen that the critical frequency was approximately 6 MHz, and the traces of the ordinary and extraordinary components, corresponding to the reflection of the radio waves from the F-region, have a normal shape. Starting at approximately 23:40 UTC, slight distortions are observed, first in the lower part of the traces (Figure 6b), and then rising up to the subcritical frequency region. These slight distortions correspond to the passage of a longitudinal wave (*P*-wave). Further, stronger distortions were observed, corresponding to the passage of a transverse wave (*S*-wave). Starting at approximately 23:51 UTC (Figures 6c and 6d), a multicusp structure, which corresponds to the Rayleigh wave, is observed on the traces.

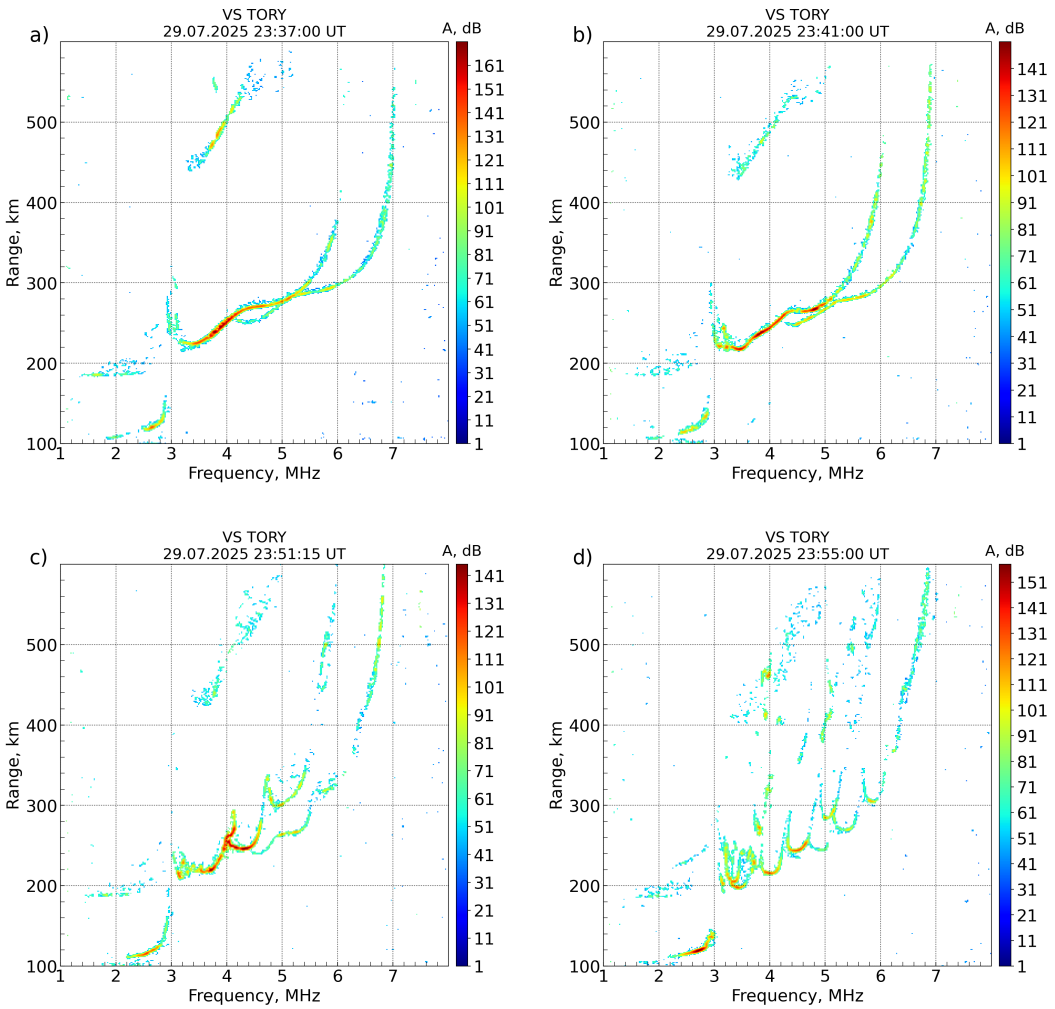

Figure 6. Vertical ionograms as obtained in Tory for individual sounding sessions.

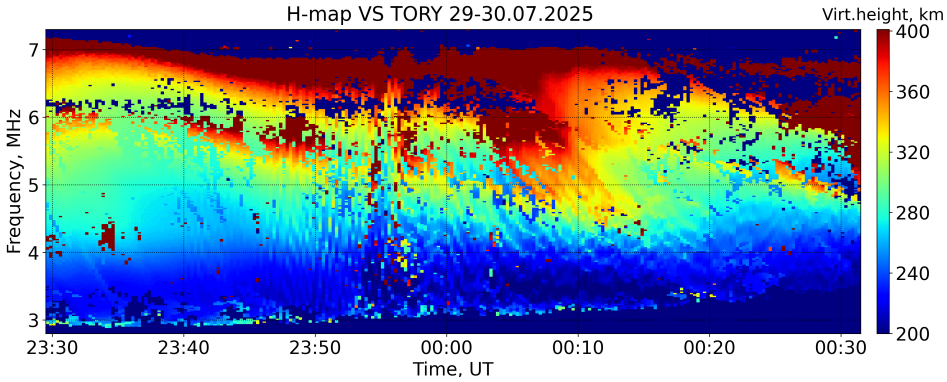

Figure 7. Virtual height map as constructed from the Tory vertical ionograms.

Figure 7 shows a virtual height map [*Yusupov et al.*, 2020]. The horizontal axis shows UTC hours, and the vertical axis shows the sounding frequency. Virtual heights are color-coded according to the color scale on the right of the map. Each vertical bar corresponds to one ionogram. To construct the map, each ionogram was subjected to secondary processing, which involved removing noise and identifying points with significant amplitude [*Ponomarchuk et al.*, 2023].

As one can see in Figure 7, until 23:40 UTC, the virtual height changes smoothly in both the frequency and time domains. After this moment, distortions in the virtual height begin to appear, manifested in alternating sections of increased and decreased heights. Individual sections can be observed moving from low to high operating frequencies. Maximum distortions are observed around 23:55 UTC and then weaken. Around this moment, it becomes noticeable that the 15-second time resolution is no longer sufficient – a distinctive strobing effect appears. The disturbed behavior of the virtual height map persisted, to varying degrees, for several hours.

Similar distortions were also observed on vertical ionograms obtained at the Klyuchi station in Novosibirsk. Figure 8a shows an undisturbed ionogram showing traces of a normal shape. The critical frequency was approximately 5 MHz. The first small distortions in the lower part of the traces began to appear at approximately 23:41 UTC (*P*-wave), and also at 23:48 UTC (*S*-wave). Then, starting at 23:54 UTC, the distortions captured the traces entirely (Figure 8b), and starting at 23:58 UTC, the distortions also took the form of the multicusp structure (Figures 8c and 8d). Figure 9 shows the corresponding virtual height map. The Novosibirsk chirp ionosonde operated with a time resolution of 1 minute, so the disturbance effect on the map is not as clearly expressed as in Figure 7. However, the basic dynamics of the distortions are repeated here, similar to what was observed in Tory.

3.4. Distortions of the Novosibirsk–Tory Oblique Ionograms

The Novosibirsk–Tory oblique sounding during the period of interest has a time resolution of 1 minute. The distance between transmitter and receiver and the azimuth are 1356 km and 96.2°, respectively. The relatively short distance allows for the recording of signals propagating via reflection from the ionospheric F-region along one-hop trajectories. The distance from the earthquake epicenter to the midpoint of the radio path (53.74°N, 93.51°E) is 4298.3 km. Figure 10a shows an oblique ionogram without disturbances, which was taken before the passage of the surface wave. The ionogram shows 1E and 1F2 traces of normal shape. Distinct effects from the passage of the infrasound wave were observed starting at 23:55 UTC. Figures 10b–d show three consecutive ionograms, revealing distortion of the 1F2 trace, caused by significant stratification of the ionospheric F2 layer near the midpoint of the radio path. It is clear that the distortions first appear on the low ray and then gradually shift to higher group paths on the high ray. Visible distortions in oblique ionograms were observed until 00:19 UTC on July 30, 2025.

Oblique ionograms recorded for the longer Magadan–Tory and Magadan–Novosibirsk radio paths (which are also shown in Figure 1 by dotted lines) during the period of interest also include the effects that can be explained by the passage of traveling ionospheric

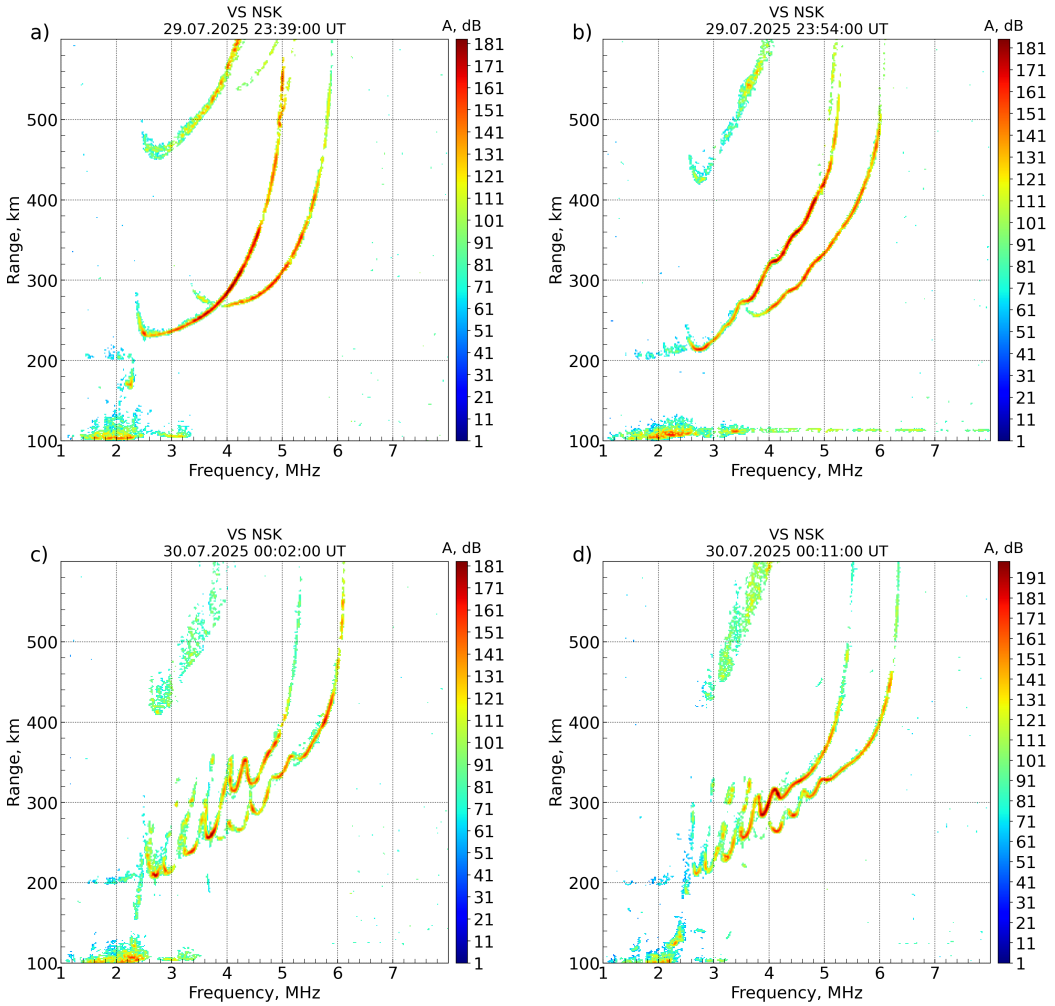

Figure 8. Vertical ionograms as obtained in Novosibirsk for individual sounding sessions.

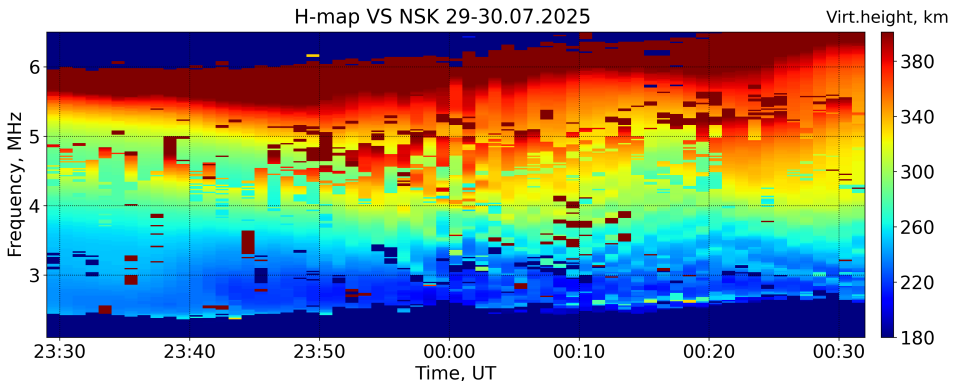

Figure 9. Virtual height map as constructed from the Novosibirsk vertical ionograms.

disturbances in the apogee of the radio wave trajectories. However, it is not possible to separate effects specifically related to the passage of the seismic wave. This can be partly explained by the lower time resolution (5 minutes), as well as by the fact that radio waves propagate along two- and three-hop trajectories.

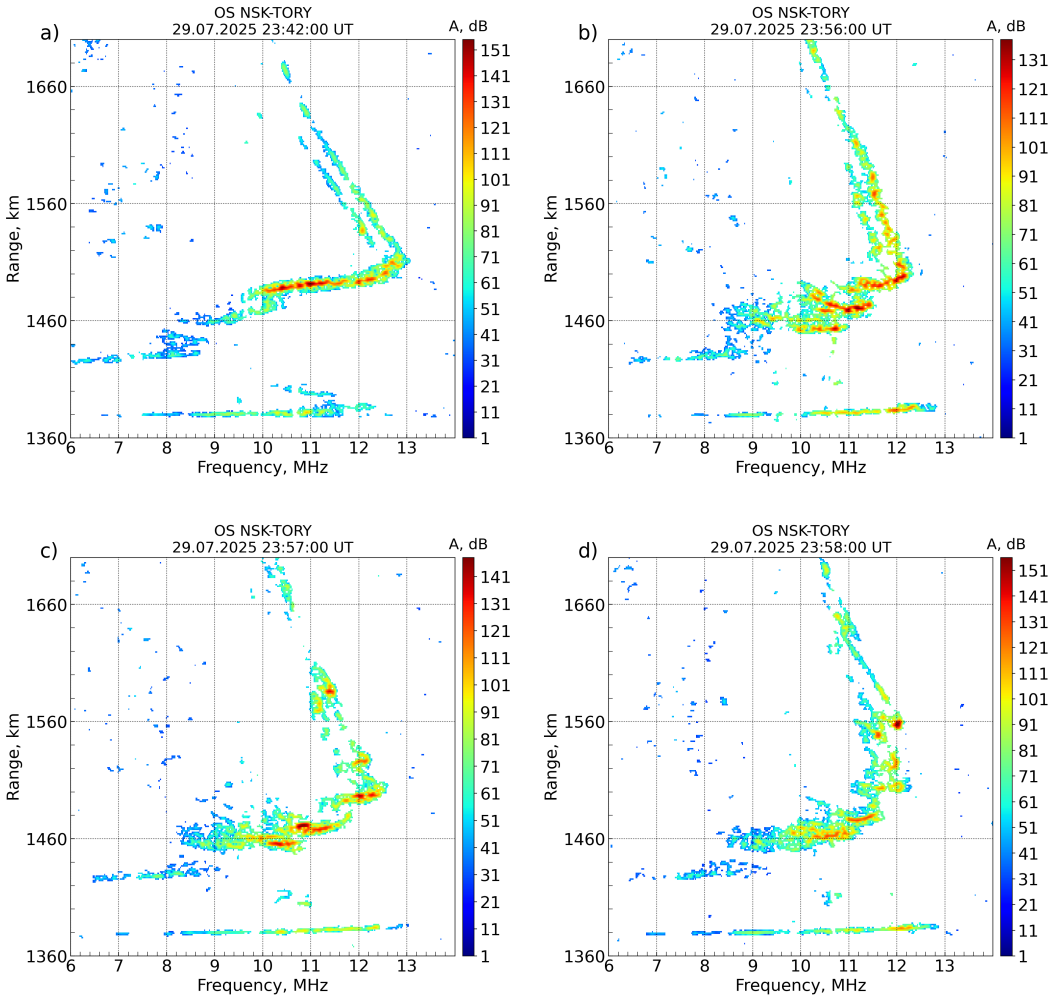

Figure 10. A series of oblique sounding ionograms along the Novosibirsk–Tory path for individual sounding sessions.

4. Discussion

The MGW HF radar data revealed variations in the ground scatter Doppler velocity. There are four inclined bands in the distance-time diagram. Within the radar's field of view, the Doppler velocity disturbances form concentric rings, the center of which roughly corresponds to the earthquake's epicenter. This suggests that the ionospheric disturbance that caused them, at F-region altitudes, propagated northwestward from the radar at a velocity of approximately 2 km/s. Similar effects were previously observed during the 2011 Tohoku earthquake using a similar SuperDARN HOK HF radar [*Nishitani et al.*, 2011; *Ogawa et al.*, 2012]. The authors detected several ionospheric disturbances (modes) propagating from the epicenter at velocities ranging from 300 m/s to 7 km/s. The high temporal resolution of one of the radar beams made it possible to record disturbances with such high velocities. Furthermore, the HOK radar is located significantly closer to the earthquake's epicenter, so its field of view also included disturbances generated directly in the epicenter region (including those resulting from impact interaction). The MGW radar's field of view is more than 1000 km from the epicenter, so the effects described here are most likely caused by the propagation of the Rayleigh wave.

Despite clear evidence that the effects observed by the MGW HF radar are caused by coseismic disturbances, questions remain regarding the correct interpretation of the data. For example, it is unclear why the velocity of the ionospheric disturbances is almost one and a half times slower than the velocity of the Rayleigh wave. Why are only four inclined bands clearly visible, and with what variations in the seismometer data (for example,

in YAK) should they be associated? A possible explanation here may be related to the peculiarities of infrasound absorption in the Earth's atmosphere, which is highly dependent on the wave frequency [*Chum et al.*, 2012]. High frequencies are absorbed more strongly than lower ones. Accordingly, only long-period components of the original infrasound signal can rise to the heights of the ionospheric maximum, where the HF radio waves are reflected. Possible inaccuracies in the mapping of the radar data, as well as their relatively low temporal and spatial resolution, complicate the interpretation. In the future, we plan to conduct comprehensive modeling of radio wave propagation characteristics, which will facilitate a more accurate interpretation and answer these questions.

Surface excess air pressure recorded at GO of ISTP SB RAS in Tory correlates well with the vertical ground oscillations at the Talaya station. The delay between the gas velocity and ground oscillations, estimated from the maximum correlation function, was ~8.86 s, and the corresponding surface wave velocity was ~3.3 km/s. A high correlation between data from the Talaya seismological station and the Tory acoustic station was previously recorded after the 2024 Taiwan earthquake [*Sorokin et al.*, 2025]. This allows us to conclude that ground motion is a direct source of infrasound waves that propagate further into the upper atmosphere, leading to modulation of the ionospheric plasma.

Distortions of traces on vertical sounding ionograms were first recorded in Tory and later at the Novosibirsk station. The trace distortions have the form of a multicusp structure, successively shifting toward higher altitudes/frequencies. This suggests that the corresponding ionospheric disturbance propagated from below upwards. The delay between seismic wave recordings at the nearest seismological stations is about 7–10 minutes and roughly corresponds to the time required for an infrasound wave to rise vertically to ionospheric altitudes. *Cedrik et al.* [2025] present the results of modeling the ionospheric response to a seismic wave after the 2024 Taiwan earthquake. A simple model was used in which the signal propagates vertically upward at the speed of sound, but the dissipation of acoustic wave energy due to viscosity and thermal conductivity is taken into account. The obtained altitude-time distributions of the disturbed electron density were then used to model the virtual height-frequency dependencies during vertical ionospheric sounding. Good qualitative agreement was demonstrated between the calculated dependencies and observed ionograms, both in terms of the shape of the distortion of the traces of the ordinary and extraordinary components, and in terms of the time of their observation. The presented results are generally consistent with those previously reported by other authors using VS data obtained after strong earthquakes [see, for example, *Maruyama and Shinagawa*, 2014; *Maruyama et al.*, 2012]. *Cedrik et al.* [2025] estimated that the vertical velocity of gas oscillations of 18 m/s at ionospheric altitudes corresponds to that of about 1 mm/s at ground-level. In the case of the Kamchatka earthquake the ground-level gas velocity is up to about 3 mm/s as seen in Figure 3b. Thus, the corresponding velocity at ionospheric altitudes should also be several times greater than estimated in *Cedrik et al.* [2025].

According to oblique ionograms taken on the Novosibirsk–Tory path, distortions of the 1F2 trace were observed, indicating significant stratification of the ionospheric F-region near the midpoint of the radio path. The high temporal resolution of the oblique ionograms suggests that the corresponding ionospheric disturbances propagated upward and were also a result of the passage of a seismic wave. The character of the distortions in the oblique ionograms suggests that the quality of HF communications could be significantly impacted.

5. Conclusion

The seismic wave generated by the earthquake near the Kamchatka Peninsula on July 29, 2025, propagated thousands of kilometers from the epicenter. Ground vibrations were consistently recorded at seismological stations located in the Asian region of Russia. As a result of ground vibrations, an infrasound wave was emitted, propagating to the ionospheric heights. Unique data on the ionospheric response to the passage of a seismic wave were obtained simultaneously using vertical, oblique, and backscatter sounding techniques

across a vast region of Asian part of Russia. Radiophysical monitoring provided information on the spatiotemporal structure of coseismic ionospheric disturbances and allowed for comparison with other observations. Acoustic monitoring confirms the mechanism by which ionospheric irregularities are formed through modulation of ionospheric plasma by an infrasound wave induced by a seismic wave.

Acknowledgments. This study was supported by the Ministry of Science and Higher Education of the Russian Federation (projects FWSE-2026-0003, FWZZ-2026-0051, and FWZZ-2026-0052). The results were obtained using the Core Shared Research Facility "Angara" of ISTP SB RAS (https://ckp-rf.ru/catalog/ckp/3056/).

References

Afraimovich E. L., Perevalova N. P., Plotnikov A. V., et al. The shock-acoustic waves generated by earthquakes // Annales Geophysicae. — 2001. — Vol. 19, no. 4. — P. 395–409. — https://doi.org/10.5194/angeo-19-395-2001

Artru J., Farges T. and Lognonné P. Acoustic waves generated from seismic surface waves: propagation properties determined from Doppler sounding observations and normal-mode modeling // Geophysical Journal International. — 2004. — Vol. 158, no. 3. — P. 1067–1077. — https://doi.org/10.1111/j.1365-246x.2004.02377.x

Berngardt O. I., Kurkin V. I., Kushnarev D. S., et al. ISTP SB RAS decameter radars // Solar-Terrestrial Physics. — 2020. — Vol. 6, no. 2. — P. 63–73. — https://doi.org/10.12737/stp-62202006

Cedrik M. V., Oinats A. V., Podlesnyi A. V., et al. Modeling of the ionosphere response to the passage of the Rayleigh wave caused by the earthquake in Taiwan on April 2, 2024 // Radio Propagation: Proceedings of the XXIX All-Russian Open Scientific Conference. — Kazan : Kazan University Press, 2025. — P. 80–83. — https://doi.org/10.26907/rwp29.2025.80-83 — (In Russian).

Chum J., Hruska F., Zednik J., et al. Ionospheric disturbances (infrasound waves) over the Czech Republic excited by the 2011 Tohoku earthquake // Journal of Geophysical Research: Space Physics. — 2012. — Vol. 117, A8. — https://doi.org/10.1029/2012ja017767

Chum J., Liu J. Y., Laštovička J., et al. Ionospheric signatures of the April 25, 2015 Nepal earthquake and the relative role of compression and advection for Doppler sounding of infrasound in the ionosphere // Earth, Planets and Space. — 2016. — Vol. 68, no. 1. — https://doi.org/10.1186/s40623-016-0401-9

Davis K. and Baker D. M. Ionospheric effects observed around the time of the Alaskan earthquake of March 28, 1964 // Journal of Geophysical Research. — 1965. — Vol. 70, no. 9. — P. 2251–2253. — https://doi.org/10.1029/jz070i009p02251

Leonard R. S. and Jr. R. A. Barnes. Observation of ionospheric disturbances following the Alaska earthquake // Journal of Geophysical Research. — 1965. — Vol. 70, no. 5. — P. 1250–1253. — https://doi.org/10.1029/jz070i005p01250

Lighthill M. J. Waves in fluids. — Cambridge, UK : Cambridge University Press, 2001.

Liu J. Y., Chen C. H., Sun Y. Y., et al. The vertical propagation of disturbances triggered by seismic waves of the 11 March 2011 M9.0 Tohoku earthquake over Taiwan // Geophysical Research Letters. — 2016. — Vol. 43, no. 4. — P. 1759–1765. — https://doi.org/10.1002/2015gl067487

Maruyama T. and Shinagawa H. Infrasonic sounds excited by seismic waves of the 2011 Tohoku-oki earthquake as visualized in ionograms // Journal of Geophysical Research: Space Physics. — 2014. — Vol. 119, no. 5. — P. 4094–4108. — https://doi.org/10.1002/2013ja019707

Maruyama T., Tsugawa T., Kato H., et al. Rayleigh wave signature in ionograms induced by strong earthquakes // Journal of Geophysical Research: Space Physics. — 2012. — Vol. 117, A8. — https://doi.org/10.1029/2012JA017952

Nishitani N., Ogawa T., Otsuka Y., et al. Propagation of large amplitude ionospheric disturbances with velocity dispersion observed by the SuperDARN Hokkaido radar after the 2011 off the Pacific coast of Tohoku Earthquake // Earth, Planets and Space. — 2011. — Vol. 63, no. 7. — P. 891–896. — https://doi.org/10.5047/eps.2011.07.003

Ogawa T., Nishitani N., Tsugawa T., et al. Giant ionospheric disturbances observed with the SuperDARN Hokkaido HF radar and GPS network after the 2011 Tohoku earthquake // Earth, Planets and Space. — 2012. — Vol. 64, no. 12. — P. 1295–1307. — https://doi.org/10.5047/eps.2012.08.001

Podlesnyi A. V., Brynko I. G., Kurkin V. I., et al. Multifunctional LFM ionosonde to the ionosphere monitoring // Heliogeophysical Research. — 2013. — Vol. 4. — P. 24–31. — (In Russian).

Pokhotelov O. A., Parrot M., Fedorov E. N., et al. Response of the ionosphere to natural and man-made acoustic sources // Annales Geophysicae. — 1995. — Vol. 13, no. 11. — P. 1197–1210. — https://doi.org/10.1007/s00585-995-1197-2

Ponomarchuk S. N., Grozov V. P. and Kotovich G. V. Technique of ionospheric parameters automatic determination from data of vertical sounding with a continuous chirp signal. — 2023. — https://doi.org/10.1117/12.2688438

Rolland L. M., Lognonné P., Astafyeva E., et al. The resonant response of the ionosphere imaged after the 2011 off the Pacific coast of Tohoku Earthquake // Earth, Planets and Space. — 2011. — Vol. 63, no. 7. — P. 853–857. — https://doi.org/10.5047/eps.2011.06.020

Sorokin A. G., Dobrynin V. A., Oynats A. V., et al. On the effect of the Rayleigh seismic wave in the atmosphere from the earthquake in Taiwan on April 3, 2024 // Collection of Proceedings of the XXXVII session of the Russian Acoustic Society. — Moscow : GEOS, 2025. — P. 84–90. — https://doi.org/10.34756/GEOS.2025.17.39225 — (In Russian).

Tsugawa T., Saito A., Otsuka Y., et al. Ionospheric disturbances detected by GPS total electron content observation after the 2011 off the Pacific coast of Tohoku Earthquake // Earth, Planets and Space. — 2011. — Vol. 63, no. 7. — P. 875–879. — https://doi.org/10.5047/eps.2011.06.035

Yusupov K. M., Mathews J. D., Maruyama T., et al. Amplitude variations of the reflected signal during vertical sounding of the ionosphere at middle latitudes // Solar-Terrestrial Physics. — 2020. — Vol. 6, no. 3. — P. 72–80. — https://doi.org/10.12737/stp-63202010